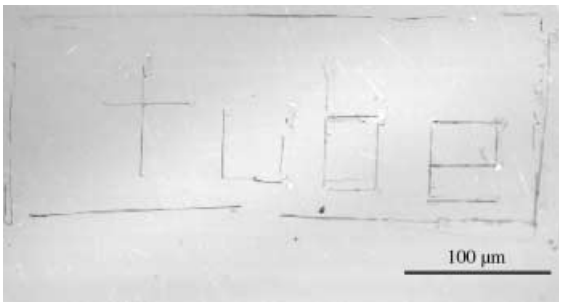

Figure 5. Confocal laser scanning micrograph of the word "tube" drawn with single nanotubes using our microinjection system. The frame, also drawn using single nanotubes, is 0.37 mm long and 0.15 mm wide. A higher magnification of this is shown in Figure 4.

manipulation easily aligns a single tube in an arbitrary direction. For demonstration we have further written the word "tube", as shown in Figure 5.

In summary, we found that the glycolipid nanotube could be a good candidate for a cytomimetic tubule in terms of its mechanical properties. Moreover, exploiting the moderate rigidity, we have developed a novel but simple aligning method: a fine line of the single nanotube is drawn freely simply by microextruding the aqueous dispersion on glass plate. Our manipulation methodology promises to open up fascinating possibilities for lipid nanotubes beyond only a substitute for microtubules; for example, a nanoneedle could be realized by extruding half of the single nanotube and fixing it at the tip of a microextrusion needle; also bridging or branching of the nanotubes on glass or metal substrates might be used as a mold for the formation of a wire and hub inside them, in molecular electronic devices; lastly, a single nanotube channel and its assembled array should provide 1D nanospace for the separation of advanced macromolecules beyond the submicro total analysis system (subμTAS).

Experimental Section

Preparation of single lipid nanotubes: These were prepared in water through self-assembly of renewable-resource-based, synthetic glycolipid cardanyl-β-D-glucopyranoside, which is a mixture of 1-*O*-3′-*n*-(8′(*Z*),11′(*Z*), 14′-pentadecatrienyl)-phenyl- β -D-glucopyranoside (ca. 29 wt%), 1-*O*-3′-*n*-(8′(*Z*),11′(*Z*)-pentadecadienyl) phenyl-β-D-glucopyranoside (ca. 16 wt%), 1-*O*-3′-*n*-(8′(*Z*)-pentadecenyl) phenyl-β-D-glucopyranoside (ca. 50 wt%), and 1-*O*-3′-*n*-(pentadecyl) phenyl-β-D-glucopyranoside (ca. 5 wt%), as reported elsewhere.[17] Nanotube structures with 10–15 nm inner diameter and high axial ratios were confirmed by TEM, field-emission scanning electron microscopy (FE-SEM), confocal laser scanning microscopy, and atomic force microscopy (AFM). On the basis of X-ray diffraction studies, the tubular membrane wall consists of three to four interdigitated lipid bilayers. Combination of a hydrogen-bond network between the glucose headgroups, π–π stacking interactions between phenyl rings, and hydrophobic interactions between long alkyl chains are responsible for the stabilization of noncovalently formed nanotube architectures.

Received: July 31, 2002 [Z19858]

[1] P. Yager, P. E. Schoen, *Mol. Cryst. Liq. Cryst. Sci. Technol., Sect. A,* **1984**, *106*, 371 – 381.
[2] J. M. Schnur, B. R. Ranta, J. V. Selinger, G. Jyothi, K. R. K. Easwaran, *Science* **1994**, *264*, 945 – 947.
[3] B. N. Thomas, C. R. Safinya, R. J. Plano, N. A. Clark, *Science* **1995**, *267*, 1635 – 1638.
[4] N. Nakashima, S. Asakuma, T. Kunitake, *J. Am. Chem. Soc.* **1985**, *107*, 509 – 510.
[5] J. H. Fuhrhop, D. Spiroski, C. Boettcher, *J. Am. Chem. Soc.* **1993**, *115*, 1600 – 1601.
[6] F. Giulieri, F. Guillod, J. Greiner, M. P. Krafft, J. G. Riess, *Chem. Eur. J.* **1996**, *2*, 1335 – 1339.
[7] S. Stewart, G. Liu, *Angew. Chem.* **2000**, *112*, 348 – 352; *Angew. Chem. Int. Ed.* **2000**, *39*, 340 – 344.
[8] P. Ringler, W. Muller, H. Ringsdorf, A. Brisson, *Chem. Eur. J.* **1997**, *3*, 622 – 625.
[9] J. H. Fuhrhop, U. Bindig, U. Siggel, *J. Am. Chem. Soc.* **1993**, *115*, 11 036 – 11 037.
[10] T. Shimizu, M. Kogiso, M. Masuda, *Nature* **1996**, *383*, 487 – 488.
[11] M. Kogiso, S. Ohnishi, K. Yase, M. Masuda, T. Shimizu, *Langmuir* **1998**, *14*, 4978 – 4986.
[12] J. M. Schnur, *Science* **1993**, *262*, 1669 – 1676.
[13] S. Iijima, *Nature* **1991**, *354*, 56 – 58.
[14] F. Gittes, B. Mickey, J. Nettleton, J. Howard, *J. Cell Biol.* **1993**, *120*, 923 – 934.
[15] H. Felgner, R. Frank, M. Schliwa, *J. Cell Sci.* **1996**, *109*, 509 – 516.
[16] M. M. J. Treacy, T. W. Ebbesen, J. M. Gibson, *Nature* **1996**, *381*, 678 – 680.
[17] G. John, M. Masuda, Y. Okada, K. Yase, T. Shimizu, *Adv. Mater.* **2001**, *13*, 715 – 718.
[18] L. A. Amos, T. S. Baker, *Nature* **1979**, *279*, 607 – 612.

Metal-Based Polyrotaxanes

Channels and Cavities Lined with Interlocked Components: Metal-Based Polyrotaxanes That Utilize Pyridinium Axles and Crown Ether Wheels as Ligands**

*Gregory J. E. Davidson and Stephen J. Loeb**

The formation of polyrotaxanes by metal–ligand self-assembly is a viable method for the programmed organization of mechanically linked molecular components into a repeating framework. This has significant potential for producing materials that contain functional molecular entities that may be addressable or controllable.[1] The challenges of designing, synthesizing, and crystallizing such materials are many and

[*] Prof. S. J. Loeb, G. J. E. Davidson
Department of Chemistry and Biochemistry
University of Windsor
Windsor, ON N9B 3P4 (Canada)
Fax: (+1) 519-973-7098
E-mail: loeb@uwindsor.ca

[**] We thank NSERC of Canada and PRF-ACS for financial support of this research. G.K.H. Shimizu and A. P. Côté of the Department of Chemistry, University of Calgary are thanked for providing the thermogravimetric analysis data.

  0044-8249/03/11501-0078 $ 20.00+.50/0

very few well-characterized examples exist.[2–6] To date, the only set of compounds to realize this combination are those prepared by Kim et al. in which a diaminoalkane "string" and cucurbituril (CB) "bead" are linked by a transition metal or lanthanide ion. This method was successfully employed to produce 1D, 2D, and 3D metal-containing polyrotaxanes,[2,3] and in one case large cavities and channels were shown to be possible.[4] In an effort to expand the number of known examples of this concept and to introduce some structural flexibility into the components, we present herein examples of metal-based polyrotaxanes constructed by using pyridinium "axles", crown ether "wheels", and transition metal ion "nodes". In particular, this design will allow investigations of some interesting concepts: 1) the effective volume of a dynamic mechanical component (crown ether) may be useful in eliminating interpenetration in metal–ligand (ML) nets[7,8] allowing the formation of large cavities, 2) the ability to change crown ethers without effecting the basic structure of a ML net could result in tremendous structural flexibility and allow the control of cavity properties and function, and 3) the dynamic motion of an interlocked component that is threaded on to an ML net may be useful in the design of addressable solid-state materials. None of these features are presently possible with known polyrotaxanes.

Scheme 1 shows how the dipyridinium axle $\mathbf{1}^{2+}$ can be threaded through dibenzo-[24]crown-8 ether, DB24C8, to produce the [2]pseudorotaxane $\mathbf{2}^{2+}$. We have previously demonstrated that this [2]pseudorotaxane can act as a ligand and that employing metal complexes as stoppers is a versatile method for producing [2]rotaxanes in good yield.[9–12] Herein, we report that this same supramolecular motif can be involved in metal–ligand self-assembly (crystal engineering) reactions and thereby be extended to polymeric systems; linear 1D and square-grid 2D metal-based polyrotaxanes.

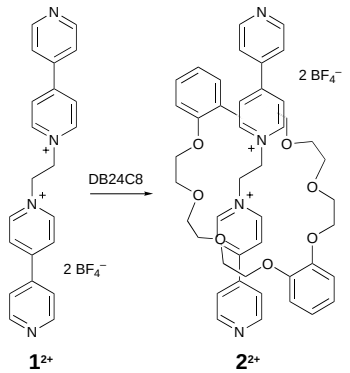

Scheme 1. The [2]pseudorotaxane $\mathbf{2}^{2+}$ is easily prepared from the dipyridinium salt $\mathbf{1}^{2+}$ and DB24C8 in a solvent such as CH_2Cl_2, acetone, MeCN, or $MeNO_2$.

One equivalent of $\mathbf{1}[BF_4]_2$ was mixed with two equivalents of DB24C8 and one equivalent of $[M(H_2O)_6][BF_4]_2$ (M = Co, Zn) in MeCN. The bulk of the solid material was isolated in good yield by reducing the volume of the mixture to about 20% of the original amount; 71% (Co), 92% (Zn). X-ray quality crystals[13] of $\{[Co(H_2O)_2(MeCN)_2(\mathbf{2})][BF_4]_4\cdot(MeCN)_2(H_2O)_2\}_x$ (**3**) were produced by slow evaporation of the

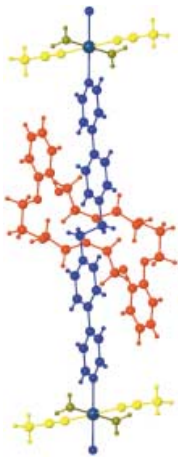

Figure 1. Ball-and-stick representation of the repeating metal–ligand unit in **3**. Key: blue: $\mathbf{1}^{2+}$ axle; red: DB24C8 wheel; dark blue: metal ion; green: H_2O; yellow: MeCN.

reaction mixture. Figure 1 shows that the use of Co^{II} ions in MeCN results in an octahedral coordination geometry comprising two [2]pseudorotaxane ligands, two MeCN molecules, and two water molecules all with *trans* orientations. The result is a 1D coordination polymer in which every bridging ligand is a [2]rotaxane. The Zn^{II} version $\{[Zn(H_2O)_2(MeCN)_2(\mathbf{2})][BF_4]_4\cdot(MeCN)_2(H_2O)_2\}_x$ (**4**) is isomorphous with **3**. Although the linker $\mathbf{1}^{2+}$ could adopt either an *anti* or *gauche* conformation at the central ethylene unit, only the *anti* conformation is possible when $\mathbf{1}^{2+}$ is threaded through a 24-membered crown ether as part of a [2]pseudorotaxane or rotaxane.[9–12,14] This combination of a *trans* geometry at the metal ion and a linear [2]pseudorotaxane ligand produces a linear 1D polymer with a repeat distance between Co atoms of 22.1 Å.

Figure 2 shows how these linear cationic 1D polyrotaxanes pack side-by-side in parallel chains in the solid state. Infinite 1D channels are formed between the polymer strands and are filled with the counterions and solvents of crystallization; in this case four BF_4^- ions, two molecules of MeCN and two molecules of water per monomer unit. Calculations

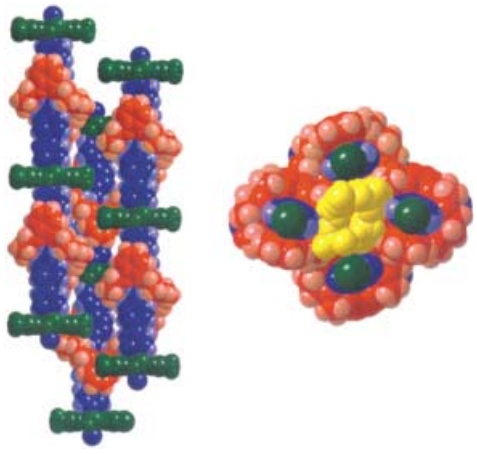

Figure 2. Space-filling representations of parallel chains of polyrotaxane **3** with solvent and anion removed for clarity (left) and a view down the chains showing the channels filled with anions and solvent (right). Key: blue: $\mathbf{1}^{2+}$ axle; red: DB24C8 wheel; green: metal with bound H_2O and MeCN ligands; yellow: anions and solvent molecules.

  0044-8249/03/11501-0079 $ 20.00+.50/0

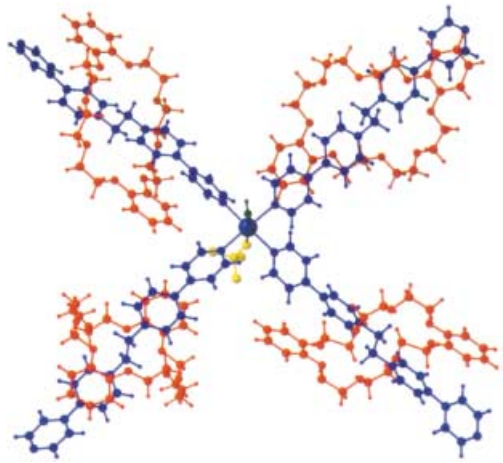

Figure 3. Ball-and-stick representation of the coordination sphere of the metal center in **5**. Key: blue: $\mathbf{1}^{2+}$ axle; red: DB24C8 wheel; green: H_2O; yellow: BF_4.

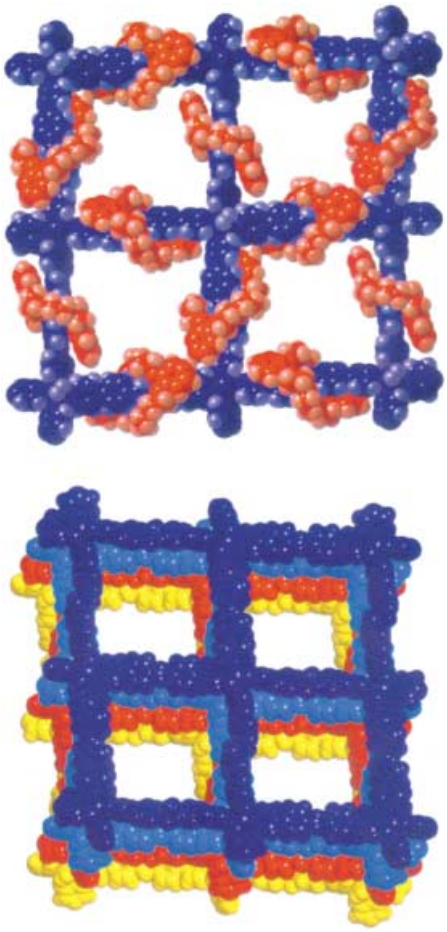

Figure 4. Top: A space-filling model showing four square-grids of **5**. ($MeNO_2$ solvent molecules and noncoordinated BF_4 anions are omitted for clarity). Key: blue: metal–ligand lattice; red = DB24C8. Bottom: Four layers of the grid are shown to emphasize the infinite channels and the open framework of the solid (DB24C8 molecules, $MeNO_2$ solvent molecules, and noncoordinated BF_4 anions are omitted for clarity).

from the X-ray structural parameters show that the accessible void space in the channels occupied by anions and solvent is 33.9%; 13.2% for solvent only.[15]

Since, the linear 1D polyrotaxanes **3** and **4** contain an octahedral metal ion in which the ancillary ligands are solvent molecules (H_2O and MeCN), we reasoned it should be possible to induce higher orders of dimensionality by employing one or a combination of noncoordinating solvents, anhydrous metal salts, and a greater amount of [2]pseudorotaxane ligand. Ultimately, we were successful in increasing the dimensionality by reacting two equivalents of $\mathbf{1}[BF_4]_2$ with four equivalents of DB24C8 and one equivalent of $[Cd(H_2O)_6][BF_4]_2$ in $MeNO_2$.[16,17] X-ray quality crystalline material was produced in good yield (>80%) by vapor diffusion of isopropyl ether into the reaction mixture. Figure 3 shows that the use of Cd^{II} ions in the noncoordinating solvent $MeNO_2$ results in an octahedral coordination geometry comprising *four* [2]pseudorotaxane ligands in a square-planar arrangement, one water molecule, and one coordinated BF_4^- anion. Figure 4 (top) shows how propagation of these units results in a 2D square net coordination polymer $\{[Cd(H_2O)(BF_4)(\mathbf{2})_2][BF_4]_5(MeNO_2)_{15}\}_x$ (**5**) in which every bridging ligand is a [2]rotaxane. The sides of the square net are defined by Cd···Cd distances of 22.2 Å, while the interlayer spacings are 12.0 and 10.0 Å, respectively, in an AB alternating pattern down the *c* axis (22.0 Å). Figure 4 (bottom) shows how this pattern gives rise to openings that are large infinite channels lined with crown ethers. These channels are not completely perpendicular to the 2D net but offset slightly as the 2D layers are knitted together by a series of H···F and H···O hydrogen bonds, which utilize the $Cd–OH_2$ unit of one layer, the neighboring $Cd–BF_4$ group in an adjacent layer, and intervening solvent molecules (there are 15 noncoordinated molecules of $MeNO_2$ per Cd^{II} ion). Calculations estimate that the accessible void space occupied by anions and solvent is 49.7%; 38.0% for solvent only.[15]

The stability of the polyrotaxane frameworks in **3**–**5** were probed by thermogravimetric analysis.[18] This showed that although the solid materials easily lost molecules of crystallization (MeCN at >70°C, H_2O at >100°C, $MeNO_2$ from 30 to 100°C) and coordinated solvent molecules (H_2O and MeCN at >150°C), the rotaxane framework did not breakdown and lose crown ether until >250°C. Presumably at this temperature, there is complete decomposition of the metal–ligand coordination polymer. This demonstrates that although the crown is initially held in position by weak noncovalent bonds in the template formation of the [2]pseudorotaxane and only interacts with the polymer by way of these residual noncovalent interactions, a covalent or strong metal–ligand bond must be broken to release this component. Therefore, incorporation of molecular machine-like units into solid-state structures by self-assembly of metal–ligand coordination polymers offers a viable route for creating functional materials and there is nothing inherently unstable about the individual rotaxane components.

From these preliminary results, we can conclude that 1) the design of open framework materials with interlocked components can be expanded to include pyridinium axles and crown ether wheels, and 2) interpenetration does not appear

  0044-8249/03/11501-0080 $ 20.00+.50/0

to be a problem as large square openings and infinite channels are possible. Further detailed experiments are needed to determine if the lack of interpenetration can be attributed to the dynamic nature of the crown units in solution and during crystallization. Future investigations will focus on the effect of changing crown ethers on the physical properties of the cavities and channels in these open framework materials.

Received: August 2, 2002 [Z19875]

[1] a) V. Balzani, A. Credi, F. M. Raymo, J. F. Stoddart, *Angew. Chem.* **2000**, *112*, 3484; *Angew. Chem. Int. Ed.* **2000**, *39*, 3348; b) A. N. Shipway, I. Willner, *Acc. Chem. Res.* **2001**, *34*, 421.

[2] K-M. Park, D. Whang, E. Lee, J. Heo, K. Kim, *Chem. Eur. J.* **2002**, *8*, 498.

[3] A dinuclear Tb^{III} center acts as the metal ion node for the 3D polyrotaxane; E. Lee, J. Heo, K. Kim, *Angew. Chem.* **2000**, *112*, 2811; *Angew. Chem. Int. Ed.* **2000**, *39*, 2699.

[4] E. Lee, J. Kim, J. Heo, D. Whang, K. Kim, *Angew. Chem.* **2001**, *113*, 413; *Angew. Chem. Int. Ed.* **2001**, *40*, 399.

[5] B. F. Hoskins, R. Robson, D. A. Slizys, *Angew. Chem.* **1997**, *109*, 2430; *Angew. Chem. Int. Ed. Engl.* **1997**, *36*, 2336.

[6] C. S. A. Fraser, M. C. Jennings, R. J. Puddephatt, *Chem. Commun.* **2001**, 1310.

[7] M. Zaworotko, *Chem. Commun.* **2001**, 1.

[8] N. G. Pschirer, D. M. Ciurtin, M. D. Smith, U. H. F. Bunz, H.-C. zur Loye, *Angew. Chem.* **2002**, *114*, 663; *Angew. Chem. Int. Ed.* **2002**, *41*, 583.

[9] S. J. Loeb, J. A. Wisner, *Chem. Commun.* **1998**, 2757.

[10] G. J. E. Davidson, S. J. Loeb, N. A. Parekh, J. A. Wisner, *J. Chem. Soc. Dalton Trans.* **2001**, 3135.

[11] a) K. Chichak, M. C. Walsh, N. R. Branda, *Chem. Commun.* **2000**, 847; b) M. J. Gunter, N. Bampos, K. D. Johnstone, J. K. M. Sanders, *New J. Chem.* **2001**, *25*, 166.

[12] Y. Diskin-Posner, G. K. Patra, I. Goldberg, *Eur. J. Inorg. Chem.* **2001**, 2515.

[13] Crystal data[19] for **3**: $C_{54}H_{72}B_4CoF_{16}N_8O_{12}$, $M_r = 1431.4$, yellow-orange blocks, ($0.28 \times 0.24 \times 0.20$ mm) monoclinic, $P2_1/c$, $a = 14.2776(1)$, $b = 11.8122(2)$, $c = 20.6360(2)$ Å, $\beta = 104.084(1)°$, $V = 3375.64(7)$ Å^3, $Z = 2$, $\rho_{calcd} = 1.408$ g cm^{-3}, $\mu = 0.360$ mm^{-1}, min/max trans. = 0.1083/0.1525, $2\theta_{max} = 50.0°$, $Mo_{K\alpha}$ $\lambda = 0.71073$ Å, $T = 293(2)$ K, 5861 total reflections (R(int) = 0.0157), $R1 = 0.0744$, wR2 = 0.2193 ($I > 2\sigma I$), $R1 = 0.0806$, $wR2 = 0.2270$ (all data), GoF (F^2) = 1.072, $N_o/N_v = 5861/440$. Crystals of **4** were of poorer quality than those obtained for **3** but the data was good enough to determine that the two structures are isomorphous with Zn replacing Co at the metal linking node. **4**: $C_{54}H_{72}B_4F_{16}N_8O_{12}Zn$, $M_r = 1437.8$, yellow blocks, ($0.24 \times 0.20 \times 0.18$ mm) monoclinic, $P2_1/c$, $a = 14.2776(1)$, $b = 11.8122(2)$, $c = 20.6360(2)$ Å, $\beta = 104.084(1)°$, $V = 3375.64(7)$ Å^3, $Z = 2$, $\rho_{calcd} = 1.415$ g cm^{-3}, $\mu = 0.469$ mm^{-1}, min/max trans. = 0.0964/0.1423, $2\theta_{max} = 42.0°$, $Mo_{K\alpha}$ $\lambda = 0.71073$ Å, $T = 293(2)$ K, 3269 total reflections (R(int) = 0.1136), $R1 = 0.1676$, $wR2 = 0.3766$ ($I > 2\sigma I$), $R1 = 0.2161$, $wR2 = 0.4140$ (all data), GoF (F^2) = 1.199, $N_o/N_v = 3269/421$. **5**: $C_{107}H_{151}B_6CdF_{24}N_{23}O_{47}$, $M_r = 3144.8$, yellow blocks, ($0.34 \times 0.26 \times 0.24$ mm) triclinic, $P\bar{1}$, $a = 17.331(2)$, $b = 20.345(2)$, $c = 22.006(2)$ Å, $\alpha = 83.692(2)$, $\beta = 80.080(2)$, $\gamma = 72.306(2)°$, $V = 7267.9(13)$ Å^3, $Z = 2$, $\rho_{calcd} = 1.437$ g cm^{-3}, $\mu = 0.269$ mm^{-1}, min/max trans. = 0.7885, $2\theta_{max} = 50.0°$, $Mo_{K\alpha}$ $\lambda = 0.71073$ Å, $T = 173.5(2)$ K, 25248 total reflections (R(int) = 0.0511), $R1 = 0.1075$, $wR2 = 0.3067$ ($I > 2\sigma I$), $R1 = 0.1431$, $wR2 = 0.3469$ (all data), GoF (F^2) = 1.345, N_o/N_v/restraints = 25248/1878/1294. Crystals of **3** and **4** were mounted on a glass fiber at room temperature, those for **5** were frozen in paratone oil inside a cryoloop. Reflection data were integrated from frame data obtained from hemisphere scans on a Bruker APEX diffractometer with CCD detector. Decay (< 1%) was monitored by 50 standard data frames measured at the beginning and end of data collection. Diffraction data and unit cell parameters were consistent with assigned space groups. Lorentzian polarization corrections and empirical absorption corrections, based on redundant data at varying effective azimuthal angles, were applied to the data sets. The structures were solved by direct methods, completed by subsequent Fourier syntheses, and refined with full-matrix least-squares methods against $|F^2|$ data. All non-hydrogen atoms were refined anisotropically. Hydrogen atoms were treated as idealized contributions. Scattering factors and anomalous dispersion coefficients are contained in the SHELXTL 5.03 program library (G. M. Sheldrick, Madison, WI). CCDC-182287 (**3**), CCDC-182288 (**4**), and CCDC-190997 (**5**) contain the supplementary crystallographic data for this paper. These data can be obtained free of charge via www.ccdc.cam.ac.uk/conts/retrieving.html (or from the Cambridge Crystallographic Data Centre, 12, Union Road, Cambridge CB21EZ, UK; fax: (+44) 1223-336-033; or deposit @ccdc.cam.ac.uk).

[14] S. J. Loeb, J. A. Wisner, *Angew. Chem.* **1998**, *110*, 3010; *Angew. Chem. Int. Ed.* **1998**, *37*, 2838.

[15] The accessible void volumes were calculated with the program PLATON by using a probe with a radius of 1.2 Å. A. M. C. T. PLATON, Utrecht University, Utrecht, The Netherlands, A. L. Spek, **1998**.

[16] Preliminary X-ray results for crystals of the Co^{II}, Ni^{II}, and Cu^{II} complexes, generated in exactly the same manner, indicate that the materials are isomorphous with **5**.

[17] **Note added in proof** (October 8, 2002): After submission of this manuscript, we determined the structure of the Cd^{II} complex in which crystals were formed under exactly the same conditions as those used to create the 2D net, but omitting the DB24C8 component. The resulting material is a 1D polymer, $\{[Cd(H_2O)_2(BF_4)_2(\mathbf{1})][BF_4]_2\}_x$, which forms a tightly packed herringbone pattern and contains no channels or cavities; details will be reported in due course.

[18] Thermogravimetric analysis were performed on a Netzsch STA449C Instrument under $N_2(g)$ atmosphere at a scan rate of 5 °C min^{-1}.

[19] Ball-and-stick and space-filling diagrams were prepared using DIAMOND-Visual Crystal Structure Information System CRYSTAL IMPACT, Postfach 1251, 53002 Bonn.

  0044-8249/03/11501-0081 $ 20.00+.50/0